

Continuous-wave terahertz spectroscopy of biotin: vibrational anharmonicity in the far-infrared

T.M. Korter, D.F. Plusquellic *

Optical Technology Division, Physics Laboratory, National Institute of Standards and Technology, 100 Bureau Dr., Gaithersburg, MD 20899-8441, USA

Received 20 October 2003; in final form 12 December 2003

Published online: 10 January 2004

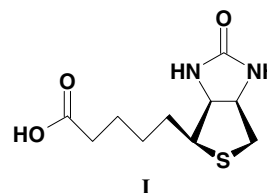
Abstract

A high-resolution continuous-wave terahertz spectrometer has been used to investigate the absorption spectrum of biotin in a polyethylene matrix from 6 to 115 cm^{-1} . Gaussian linewidths from least squares fits at 4.2 K are found to increase from 1 to 5 cm^{-1} over this region establishing conservative lower limits on the vibrational lifetimes from 5 to 1 ps. The calculated partition function of 1.0 at 4.2 K is shown to increase to $>10^8$ at 298 K indicating enormous changes in the sequence level populations with increasing temperature. Lineshape models that include mechanical anharmonicity were therefore necessary to obtain satisfactory fits at 298 K. Anharmonicity factors ($\chi_e \bar{\nu}_e / \bar{\nu}_e$) range from 0.1% to 1% and establish their importance for refining model predictions.

Published by Elsevier B.V.

1. Introduction

The spectrum of terahertz (THz) radiation is well matched to the low-frequency motions important for the flexibility and thus the function of many biological molecules. The large-amplitude vibrational modes probed in THz spectroscopy provide insight into the structural dynamics of biomolecules by directly interrogating the motions responsible for conformational isomerization. These low-frequency modes are most conveniently investigated on small molecular systems where the individual resonances can be spectrally resolved and potentially assigned to a nuclear motion with the aid of molecular modeling. We have chosen to investigate the low-frequency vibrations of the small biomolecule, biotin (I), in an effort to better understand the conformational flexibility responsible for its bioactivity.



Large-amplitude motions play a critical role in the function of biotin, a vitamin coenzyme that catalyzes carboxylation and decarboxylation reactions [1] by aiding transport of intermediates between the two active sites of pyruvate carboxylase. The THz spectrum of biotin was acquired to obtain information about the low-frequency vibrations that form the basis for this transport motion. Conformational minima from the torsional motion of the side chain alone number more than 100. The frequencies and absorption intensities of transitions in the THz spectrum yield information about the vibrations and conformations of this highly flexible molecule.

Continuous-wave THz linear-absorption spectroscopy is well suited for the investigation of low-frequency vibrational motions. Terahertz radiation

* Corresponding author. Fax: +1-3019752950.

E-mail address: david.plusquellic@nist.gov (D.F. Plusquellic).

produced by pumping solid-state photomixers with continuous-wave, near-infrared laser sources, offers several advantages over blackbody and pulsed-laser THz sources. These advantages include a narrow spectral bandwidth (limited by the two pump laser line widths), excellent frequency control, and intensity stability, all of which are important for signal averaging and for monitoring line intensities. Moreover, the bulky pump lasers can be easily isolated from the compact THz source by the use of optical fibers for the propagation of the near-infrared pump laser beams to the photomixer. Such remote operation is convenient for performing THz measurements at sites removed from the laser facility, for coupling to certain sample systems, and for minimizing the propagation of the THz radiation through the atmosphere where it is strongly absorbed by water vapor.

2. Experiment

A diagram of the continuous-wave THz laser spectrometer is shown in Fig. 1. Continuous-wave (CW) THz radiation is generated by the difference-frequency mixing of two near-infrared (≈ 850 nm) lasers at the surface of a solid-state photomixer. The photomixer consists of epitaxial low-temperature-grown GaAs (LT-GaAs) on a GaAs substrate. The LT-GaAs layer is topped by submicron interdigitated gold-on-titanium electrodes, which are coupled to a self-complementary spiral antenna for broad-band output [2]. The photomixer has an $8 \mu\text{m} \times 8 \mu\text{m}$ central region containing

eight $8 \mu\text{m} \times 0.2 \mu\text{m}$ electrodes separated by $0.8 \mu\text{m}$. The front surface is antireflection coated for 850 nm. The photomixer is operated at room temperature and biased with a voltage from 15 to 20 V. The physical properties and performance characteristics of these types of photomixers have been given in detail elsewhere [3–5] and their application to THz spectroscopy has been previously demonstrated [6,7].

The two near-infrared pump lasers consist of an amplified diode laser and an Ar^+ -pumped CW Ti:Sapphire ring laser. The diode laser is operated near 850 nm and seeds an amplifier that produces approximately 500 mW of output power. Two optical isolators (>60 dB isolation) between the diode and amplifier limit optical feedback, thus aiding in the greater than $1000:1$ suppression of power in other laser modes. The Ti:Sapphire laser generates >500 mW of power. Both lasers are attenuated to 20 mW to prevent damage to the photomixer, combined on a 50% beamsplitter, and mechanically chopped at 300 Hz prior to coupling into a single-mode fiber for propagation to the photomixer. The output light from the fiber is free-space propagated for approximately 25 cm and tightly focused onto the $8 \mu\text{m} \times 8 \mu\text{m}$ active region of the photomixer using a 1.9 cm focal length aspheric lens. A $\lambda/2$ wave plate in the Ti:Sapphire beam prior to the beam splitter allows optimization of the polarization alignment at the photomixer.

A silicon hemispherical lens is optically contacted to the backside of the photomixer to generate a quasi-Gaussian THz beam [8]. No other transmissive-type optics are used to minimize absorption loss and interference effects at the detector from surface reflections. The THz beam is propagated by means of four parabolic gold mirrors each having a 7.6 cm effective focal length. The first two mirrors collect, collimate, and re-focus the THz beam onto the cryogenic sample to a beam waist of approximately 1 mm at 1 THz. The second two mirrors image this spot onto a liquid-He-cooled silicon composite bolometer detector fitted with a $20 \mu\text{m}$ low-pass optical filter. The detector with preamplifier has a 3 dB bandpass at 1 kHz. A 5 mm thick Teflon flat serves as the entrance window to the bolometer during sample alignment and is removed from the beam path during acquisition of data.

The Ti:Sapphire laser is tuned via a computer interfaced stepper motor driving an intracavity Lyot filter. No other intracavity frequency narrowing elements are used. Consequently, the step frequency resolution of the THz spectrometer is limited to approximately 0.1 cm^{-1} although a much higher resolution of 0.0001 cm^{-1} is possible. Typically, spectra are acquired from 0.1 to 3.5 THz by scanning the Ti:Sapphire laser from 11760 to 11874 cm^{-1} with the diode laser locked to the reference cavity near 11757 cm^{-1} . The frequency calibration of the THz spectra is performed by recording wavemeter

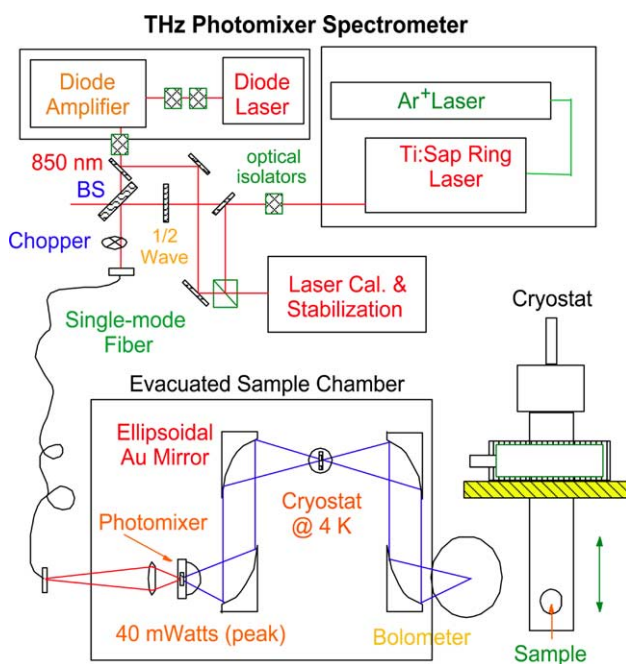


Fig. 1. A schematic diagram of the photomixer laser spectrometer operational from 0.1 to 4 THz.

readings of the Ti:Sapphire laser at 0.1 cm^{-1} resolution during the course of a scan. Above 3.5 THz, bolometric detection of the thermal radiation from pump laser heating of the photomixer is comparable to the THz power generated. Cryogenic cooling of the photomixer to 77 K is expected to reduce this background signal while improving the conversion efficiency of the photomixer [9].

Evacuation of the entire optical system serves two purposes. Cryogenic cooling to 4.2 K removes spectral congestion from vibrational sequence levels and combination bands and results in drastic population increases of the lowest energy vibrational and conformational states of the molecules. Also, the severe absorption by water vapor is eliminated from the optical path.

Pressed disks of polyethylene of equal thickness (0.4 cm) with and without dry samples of biotin (50 mg of biotin in 500 mg of polyethylene or 10% by weight) were prepared using a 1.26 cm round pellet press. High-density polyethylene is used as a sample matrix due to its transparency in the THz region. The two polyethylene pellets, one with sample and one without sample, are inserted side-by-side into a holder and cooled to 4.2 K in a temperature regulated cryostat. Terahertz laser scans of the sample and the polyethylene blank are done consecutively after interchanging the two samples by simple elevation of the cryostat, to minimize instrumental artifacts from changes in standing wave patterns. Lock-in signals of the bolometer and photocurrent (measured as a voltage across a 100Ω shunt) are digitized concurrently at 100 Hz with a time constant of 30 ms. Both the sample and blank are normalized to the photocurrent signal (after subtracting off the DC current offset) to correct for laser-power variations. The normalized data are signal averaged and mapped onto a scale of constant wavenumber spacing. Finally, sample data are normalized to the polyethylene blank and converted to absorbance (base 10).

3. Results and discussion

Terahertz absorption spectra of biotin in a polyethylene matrix are shown in Fig. 2 from 0.2 to 3.5 THz. The top and bottom spectra correspond to 4.2 and 298 K, respectively. A gradual rise of the absorption baseline with increasing frequency appears in both spectra possibly resulting from Mie scattering over the decade change in the THz wavelength or from broad unstructured absorption features of biotin. The 4.2 K spectrum contains several discrete resonance features having Gaussian linewidths that range from 1 cm^{-1} at 18 cm^{-1} to 5 cm^{-1} at 100 cm^{-1} . Remarkably, these same resonances are identifiable in the room temperature spectrum, although are somewhat broader and generally red-shifted.

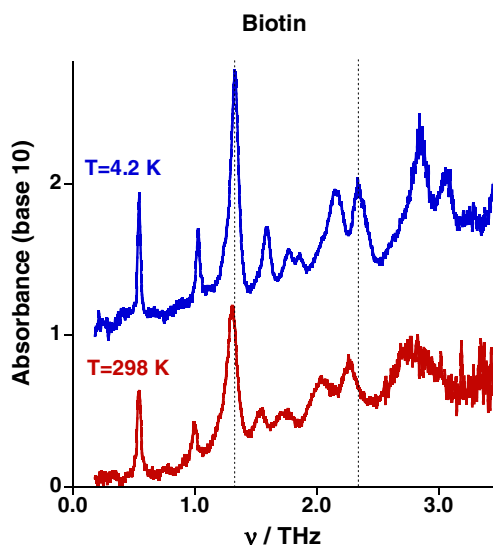


Fig. 2. The THz absorption spectra of biotin obtained at 298 K (lower trace) and at 4.2 K (upper trace) in a polyethylene matrix. The 0.4 cm thick sample contained 50 mg of biotin in 500 mg of polyethylene. The dashed lines illustrate the relative shifts of the peak absorbance of features at 1.3 and 2.3 THz at the two temperatures. The 4.2 K spectrum is offset for clarity.

Many factors may contribute to the absorption widths of samples embedded in a polyethylene matrix. Line broadening mechanisms may include inhomogeneous effects arising from differences in the local environment and homogeneous broadening from rapid collisional dephasing and vibrational energy exchange between molecules (both biotin and polyethylene). The temperature dependence of the vibrational frequencies and linewidths may result from structural changes in the matrix cage, from mechanical anharmonicity in the vibrational force field, from electrical anharmonicity in the transition dipole moment function and/or from increases in the rates of dephasing and energy exchange with increasing available energy.

Vibrational spectra in the THz region are uniquely sensitive to temperature. Excitation energies are typically much less than the available room temperature thermal energy of 210 cm^{-1} (6.2 THz), resulting in substantial thermal population in excited vibrational states. Consequently, room temperature absorption spectra are not only a measure of the fundamental band ($v = 1 - 0$), but also sequence bands, $v = 2 - 1$, $3 - 2$, etc. The anharmonicities of the potential energy surfaces may be investigated by examining the temperature dependence of these spectra. For example, a vibrational mode with a fundamental frequency of 33 cm^{-1} (1 THz) will have, ignoring anharmonicity, thermal population in excess of 1% in levels up to $v = 18$. Positive (negative) mechanical anharmonicity in the potential leads to a decrease (increase) in the vibrational level spacing with increasing vibrational quanta. When the sequence level structure is not resolved, lineshapes will broaden and

distort asymmetrically towards lower (higher) frequencies. Cryogenic cooling to a liquid He temperature of 4.2 K will have a drastic effect on sequence level structure. For frequencies greater than 1 THz, the vibrational zero-point level will have more than 99% of the total thermal population. Therefore, absorption features represent only the fundamental vibrational modes. In principle, comparisons of spectra taken at these two temperatures provide a sensitive means to quantify the mechanical anharmonicity of the potential energy surfaces.

As evident from comparison of the relative frequencies and peak absorbances in Fig. 2, most of the room temperature features are broadened and red-shifted relative to those at 4.2 K. The magnitudes of the red shifts increase approximately linearly with frequency suggesting that mechanical anharmonicity may likely account for these trends [10]. To explore this possibility further, the following model has been applied to account for the observed temperature dependence of these spectra. For this analysis, we assume other sources of line broadening are insignificant. Therefore, these results represent upper limits on the magnitudes of the mechanical anharmonicity. We further assume that the electric dipole moment is a linear function of the displacements from equilibrium, i.e., the electrical anharmonicity is zero.

The mechanical anharmonicity, χ_e of a vibrational mode, q , with harmonic frequency, $\bar{\nu}_e$, is given in its simplest form by the energy levels, m , of a Morse oscillator

$$\bar{\nu}_m = (m + 1/2)\bar{\nu}_e^{(q)}[1 - \chi_e(m + 1/2)]. \quad (1)$$

The peak absorption coefficient [11], $\kappa^{(q)}(\bar{\nu})$, in units of cm^{-1} is

$$\kappa^{(q)}(\bar{\nu}) = \frac{8\pi^3 N}{3h\Theta^{(q)}} \sum_{m=0}^{\infty} \bar{\nu}_{m+1,m} \cdot e^{-\frac{\bar{\nu}_{m,0}}{k_b T}} \left[1 - e^{-\frac{\bar{\nu}_{m+1,m}}{k_b T}} \right] \left| \mu_{m+1,m}^{(q)} \right|^2 \gamma(\bar{\nu}). \quad (2)$$

Here, N is the total number of molecules/ cm^3 , $\mu_{m+1,m}^{(q)}$ is the transition dipole moment, T is the temperature, k_b is the Planck's constant ($0.6950356 \text{ cm}^{-1} \text{ K}^{-1}$), c the speed of light and

$$\bar{\nu}_{m+1,m} = \bar{\nu}_{m+1} - \bar{\nu}_m, \quad (3)$$

$$\gamma(\bar{\nu}) = \sqrt{\frac{4 \ln 2}{\pi \cdot \Delta \bar{\nu}_{\text{FWHM}}^2}} e^{-\frac{4 \ln 2 (\bar{\nu} - \bar{\nu}_{m+1,m})^2}{\Delta \bar{\nu}_{\text{FWHM}}^2}}, \quad (4)$$

$$\Theta^{(q)} = \sum_{m=0}^{\infty} e^{-\frac{\bar{\nu}_{m,0}}{k_b T}} = \left[1 - e^{-\left(\frac{\bar{\nu}_e^{(q)}}{k_b T}\right)} \right]^{-1}, \quad (5)$$

where $\gamma(\bar{\nu})$ is a normalized Gaussian function with width, $\Delta \bar{\nu}_{\text{FWHM}}$ and $\Theta^{(q)}$ is the vibrational partition

function with the last equality valid in the harmonic limit only. The squared transition dipole matrix elements for a harmonic oscillator are

$$\left| \mu_{m+1,m}^{(q)} \right|^2 = \left| \mu_e^{(q)} \right|^2 \cdot \frac{h}{8\pi^2 c \bar{\nu}_e^{(q)}} (m + 1), \quad (6)$$

while those derived from perturbation theory that include corrections to the fundamental intensity up to second order have the form [12]

$$\left| \mu_{m+1,m}^{(q)} \right|^2 = \left| \mu_e^{(q)} \right|^2 \cdot \frac{h}{8\pi^2 c \bar{\nu}_e^{(q)}} [(m + 1) - 2\chi_e^{(q)}(m + 1)^2]. \quad (7)$$

Finally, we also consider the squared matrix elements of a Morse oscillator which have been given before [13]. In mass weighted coordinates, these elements are

$$\left| \mu_{m+1,m}^{(q)} \right|^2 = \left| \mu_e^{(q)} \right|^2 \cdot \frac{h}{8\pi^2 c \bar{\nu}_e^{(q)} \chi_e^{(q)}} \cdot \frac{1}{(L - 2m - 2)^2} \cdot \left[\frac{(m + 1)(L - 2m - 1)(L - 2m - 3)}{L - m - 1} \right], \quad (8)$$

where $L = 1/\chi_e^{(q)}$. It is easily verified in Eqs. (7) and (8) that as $\chi_e^{(q)}$ approaches zero, the matrix elements of Eq. (6) are obtained. For this analysis, only transitions with $\Delta m = +1$ are considered since overtone absorption intensities are typically an order-of-magnitude weaker than the fundamental.

Eq. (2) ignores contributions from combination bands. However, in the absence of Fermi resonance interactions and/or anharmonic coupling between modes, it is easily shown from the laws of exponents that Eq. (2) gives the correct answer, i.e.

$$\begin{aligned} & \frac{\sum_{m=0}^{\infty} e^{-\frac{\bar{\nu}_{m,0}}{k_b T}} \left[1 - e^{-\frac{\bar{\nu}_{m+1,m}}{k_b T}} \right]}{\Theta^{(q)}} \\ &= \frac{\prod_{r \neq q \neq s=1}^{3n_{\text{atoms}}-6} \Theta^{(r)} \sum_{n=0}^{\infty} e^{-\frac{\bar{\nu}_{n,0}}{k_b T}} \sum_{m=0}^{\infty} e^{-\frac{\bar{\nu}_{m,0}}{k_b T}} \left[1 - e^{-\frac{\bar{\nu}_{m+1,m}}{k_b T}} \right]}{\Theta^{(T)}} \\ &= \frac{\prod_{r \neq q \neq s=1}^{3n_{\text{atoms}}-6} \Theta^{(r)} \sum_{n=0}^{\infty} \sum_{m=0}^{\infty} e^{-\left(\frac{\bar{\nu}_{m,0}}{k_b T} + \frac{\bar{\nu}_{n,0}}{k_b T}\right)} \left[1 - e^{-\frac{\bar{\nu}_{m+1,m}}{k_b T}} \right]}{\Theta^{(T)}}, \quad (9) \end{aligned}$$

and likewise for all combinations with the remaining modes, r , that contribute to the total vibration partition function, $\Theta^{(T)}$. Under these conditions, the integrated intensity of a given line must be conserved since all sets of sequence transitions overlap and probe the total vibrational state population independent of temperature.

Applications of these models to the absorption spectra of biotin from 5 to 115 cm^{-1} are illustrated in Fig. 3. The linearly increasing baseline has been subtracted from the 4.2 K (top trace) and the room tem-

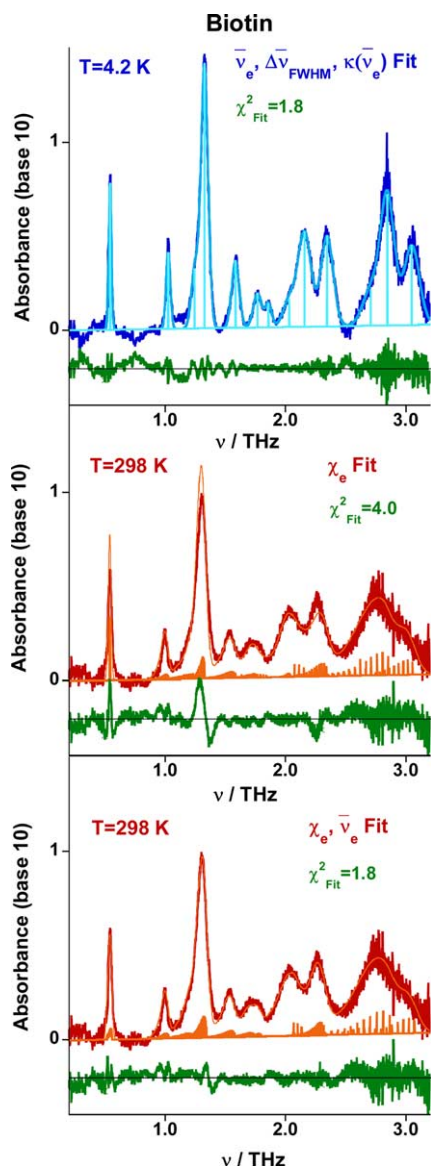


Fig. 3. Results from non-linear least squares fits to lineshape models based on Eq. (2). The 4.2 K spectrum is shown in the top panel and is overlaid with the best-fit simulated spectrum. In each panel, residuals are shown as the lowest trace and the center frequency and peak absorbance of each calculated transition is shown with a stick. The 298 K spectrum is shown in both the middle and lower panels. The anharmonicity factors, χ_e , were the only parameters varied for the simulated spectrum in the middle panel. The parameters $\bar{\nu}_e$, $\kappa(\bar{\nu}_e)$ and $\Delta\bar{\nu}$ were held fixed at the 4.2 K values. The simulated spectrum shown in the lower panel is similar except that $\bar{\nu}_e$ was also permitted to vary for each of the 13 features. Notice the large number of sequence transitions contributing to the absorbance at 298 K.

perature spectrum (middle and lower traces) to aid in comparison with these predictions. In the top panel are shown the minimum number of Gaussian peaks required to account for all of the observed features at 4.2 K. The 13 transitions identified were included in a non-linear least squares fit of the harmonic frequencies, $\bar{\nu}_e$, Gaussian linewidths, $\Delta\bar{\nu}_{\text{FWHM}}$ and peak absorbances, $\kappa(\bar{\nu}_e)$, using features of the *JB95* software [14]. Since the

room temperature spectra are most sensitive to anharmonicity, the 4.2 K parameters were used in fits of the room temperature spectrum by varying only the anharmonicity factors, χ_e . These factors were included in refits at 4.2 K and this procedure was repeated until self-consistent parameters were obtained in both spectra.

The transition dipole matrix elements of a Morse oscillator given by Eq. (8) were used for the final fits to Eq. (2). The anharmonicity factors changed by less than 5% when using either the harmonic expression of Eq. (6) or those derived from perturbation theory in Eq. (7). These changes are typically less than the experimental uncertainty in the parameters. Furthermore, the integrated intensity over each set of sequence levels is conserved at the two temperatures as required by Eq. (9). (Contributions at 298 K even include intensity from combination bands with fundamental frequencies outside of the scanned region.) Based on the 13 features identified, the calculated partition function at 4.2 K is 1.0 and increases to 1.5×10^8 at 298 K. This drastic increase in the number of microstates establishes credibility to the assumptions made in Eq. (9) since otherwise, the room temperature features would be completely unresolved. The best fit simulated spectra are overlaid with the experimental data in the top and middle panels of Fig. 3. The vibrational frequencies and peak absorbances used in this model are shown as sticks in the figure. The residuals are also shown to illustrate the quality of the fit.

While this model accounts for the vast majority of the temperature-dependent features in the spectrum of biotin, there appears to be some discrepancy with experiment near the shoulders of some lines. Along with the drastic changes in sequence level populations, the decrease in temperature might reasonably affect the dimensions of the polyethylene and/or biotin cages and consequently, result in small shifts of the harmonic frequencies. To account for such shifts, refits of the room temperature spectra were performed by varying both the anharmonicity factors and the harmonic frequencies. The best fit lineshapes are shown in the bottom panel of Fig. 3. The χ^2 residual of the fit is now similar to that obtained at 4.2 K.

The parameters obtained from the fits are given in Table 1. The uncertainties reported are type A and represent one standard deviation of the parameters. The observed widths at 4.2 K range from 1 cm^{-1} at 20 cm^{-1} to 5 cm^{-1} at 100 cm^{-1} . Vibrational lifetimes ranging from 5 to 1 ps over this interval therefore represent conservative lower limits if the fitted lineshape functions were pure Lorentzian. Interestingly, these observed widths increase in proportion to frequency. The constant ratio is consistent with an inhomogeneous broadening mechanism where each subset of molecules experience slightly different local environments. This is in contrast

Table 1

Harmonic frequencies ($\bar{\nu}_e$), peak absorption coefficients [$\kappa(\bar{\nu}_e)$], Gaussian linewidths ($\Delta\bar{\nu}_{\text{FWHM}}$), shifts (δ) and anharmonicity constants (χ_e) of biotin obtained from non-linear least squares fits of spectra obtained at 4.2 and 298 K. Type A standard uncertainties (i.e., $k = 1$ or 1σ) are given, as determined directly from the least-squares fit

	4 K			298 K	298 K	
	$\bar{\nu}_e$ (cm ⁻¹)	$\kappa(\bar{\nu}_e)^a$ (cm ⁻¹)	$\Delta\bar{\nu}$ (cm ⁻¹)	χ_e^b	δ^c (cm ⁻¹)	χ_e^d
1	18.12(5)	1.95(8)	0.92(1)	0.00010(4)	-0.57(5)	0.00097(4)
2	34.34(5)	1.00(8)	1.4(1)	0.0017(5)	+0.04(5)	0.0017(6)
3	41.85(5)	0.77(5)	2.2 ^e	0.0041(6)	-0.33(5)	0.0040(4)
4	44.44(5)	3.50(7)	2.4(1)	0.0015(7)	+0.61(5)	0.0022(3)
5	53.22(5)	0.87(4)	2.4(1)	0.0035(5)	-0.27(5)	0.0033(5)
6	59.31(7)	0.45(4)	2.7(2)	0.0031(8)	-1.20(5)	0.0032(4)
7	62.20(10)	0.30(3)	2.1(2)	0.0070(9)	-2.18(5)	0.0018(4)
8	68.20(10)	0.30(3)	4.0 ^e	0.0013(7)	+1.39(5)	0.003 ^e
9	73.19(5)	1.25(7)	4.3(1)	0.0090(6)	-0.78(5)	0.0078(8)
10	78.72(5)	1.20(9)	4.0(1)	0.0043(7)	-0.98(5)	0.0031(7)
11	91.80(40)	0.47(5)	5.3(5)	0.008 ^e	+1.16(5)	0.008 ^e
12	96.71(7)	1.72(8)	4.6(1)	0.0080(8)	+0.68(5)	0.0092(6)
13	103.2(1)	1.05(8)	5.0(1)	0.0062(8)	+0.75(5)	0.0074(5)

^a Peak absorption coefficients per cm pathlength (base 10) from Eq. (2).

^b Anharmonicity factors from fit with $\bar{\nu}_e$, $\kappa(\bar{\nu}_e)$ and $\Delta\bar{\nu}$ fixed at the 4.2 K values.

^c Best-fit harmonic frequencies at 298 K, specified as shifts: i.e., $\bar{\nu}_e$ (298 K) - $\bar{\nu}_e$ (4.2 K).

^d Same as in footnote b except the harmonic frequencies, $\bar{\nu}_e$, were also varied.

^e Parameter fixed in the fit at a reasonable value based on the trends.

to a homogeneous mechanism where non-linear scaling of Lorentzian widths might be expected with frequency-dependent changes in the density of states and squared magnitudes of the coupling matrix elements. Somewhat anomalous, however, is the trend in the anharmonicity factors, χ_e , which for the most part is seen to increase with frequency. One possible explanation might be that with increasing frequency, the vibrational motions become more 'local-mode-like' and therefore, would be more strongly influenced by the degree of intermolecular hydrogen bonding. Additional support for this reasoning comes from the finding that all anharmonicity factors are positive suggesting that the observed modes involve intermolecular stretching modes and not intramolecular torsional motions which would likely have negative anharmonicity factors. No such trends are found, however, in the frequency shifts which have both positive and negative values at room temperature.

4. Summary and conclusions

A continuous-wave THz spectrometer has been constructed for high-resolution investigations of the lowest frequency vibrations of biomolecules in condensed phases. The THz spectrum of biotin has been obtained from 0.2 to 3.5 THz. The spectrum of biotin displays several resolved absorption features at both 4.2 K and room temperature. Vibrational anharmonicity adequately accounts for observed line shapes over this temperature range suggesting other sources of line broadening are small in comparison. Anharmonicity factors ($\chi_e \bar{\nu}_e / \bar{\nu}_e$) at the levels from 0.1% to 1.0% are fit to

the observed lineshapes at room temperature and illustrate their importance for refining model predictions. While the majority of the temperature-dependent features are explained by this model, the room temperature fit is further improved if small center frequency shifts are permitted which presumably accounts for size changes in the crystalline cage environment with temperature.

Acknowledgements

We acknowledge Angela Hight Walker, Christine Bucher, Gerald T. Fraser and Richard D. Suenram at NIST for helpful discussions.

References

- [1] L. Stryer, *Biochemistry*, fourth edn., W.H. Freeman, New York, 1995 (Chapter 9).
- [2] K.A. McIntosh, E.R. Brown, K.B. Nichols, O.B. McMahon, W.F. DiNatale, T.M. Lyszczarz, *Appl. Phys. Lett.* 67 (1995) 3844.
- [3] S. Verghese, K.A. McIntosh, E.R. Brown, *Appl. Phys. Lett.* 71 (1997) 2743.
- [4] E.R. Brown, *Appl. Phys. Lett.* 75 (1999) 769.
- [5] S.M. Duffy, S. Verghese, K.A. McIntosh, A. Jackson, A.C. Gossard, S. Matsuura, *IEEE Trans. Microwave Theory Tech.* 49 (2001) 1032.
- [6] A.S. Pine, R.D. Suenram, E.R. Brown, K.A. McIntosh, *J. Mol. Spectrosc.* 175 (1996) 37.
- [7] S. Matsuura, P. Chen, G.A. Blake, J.C. Pearson, H.M. Pickett, *IEEE Trans. Microwave Theory Tech.* 48 (2000) 380.
- [8] A. Gurtler, C. Winnewisser, H. Helm, P.U. Jepsen, *J. Opt. Soc. Am. A* 17 (2000) 74.
- [9] S. Verghese, K.A. McIntosh, E.R. Brown, *Appl. Phys. Lett.* 71 (1997) 2743.

- [10] M. Walther, P. Plochocka, B. Fischer, H. Helm, P. Uhd Jepsen, *Biopolymers* 67 (2002) 310.
- [11] E.B. Wilson Jr., J.C. Decius, P.C. Cross, *Molecular Vibrations: The Theory of Infrared and Raman Vibrational Spectra*, McGraw-Hill, New York, 1955.
- [12] B.L. Crawford Jr., H.D. Dinsmore, *J. Chem. Phys.* 18 (1950) 983.
- [13] J.A.C. Gallas, *Phys. Rev. A* 21 (1980) 1829.
- [14] D.F. Plusquellic, R.D. Suenram, B. Maté, J.O. Jensen, A.C. Samuels, *J. Chem. Phys.* 115 (2001) 3057.